Mine Water Environ
DOI 10.1007/s10230-013-0223-y

TECHNICAL ARTICLE

Modified Multi-phase Stability Diagrams: An AMD Case Study at a Site in Northumberland, UK

Katarzyna Samborska · Sławomir Sitek · Simon H. Bottrell · Ondra Sracek

Received: 22 June 2012 / Accepted: 1 March 2013

Abstract The weathering of sulphide minerals within spoil heaps causes the release of sulphate and environmentally hazardous metal ions. Newly-formed species can subsequently precipitate as highly soluble, secondary sulphate minerals, which, in turn, might be flushed by dilute recharge water or eventually transformed into more stable minerals. These processes determine which components are retained in the spoil as immobile solid phases and which (and when) others are released into the wider aquatic environment. To elucidate this sequence of mineral formation and transformation, we studied mineral-fluid equilibria in a major abandoned coal mine spoil heap at the former Shillbottle Colliery, Northumberland, UK. The investigations focussed on stability of iron minerals produced during the acid mine drainage process. The multi-component Phreeplot-calculated pE/pH diagrams reveal that many post-mining secondary minerals may co-exist, in contrast to what is indicated by the more commonly used charts. Being able to visualize the mutual stability of these minerals under specific chemical and physical conditions might aid understanding of formation and transformation mechanisms.

Keywords Acid mine drainage · Iron · Phreeplot · pE/pH diagrams · Shillbottle Colliery

K. Samborska (✉)
Institute for Ecology of Industrial Areas,
6 Kossutha Str, 40-844 Katowice, Poland
e-mail: samborska@ietu.katowice.pl

S. Sitek
Department of Hydrogeology and Engineering Geology,
University of Silesia, 41-200 Sosnowiec, Poland

S. H. Bottrell
Earth Surface Sciences Institute,
School of Earth and Environment,
University of Leeds, Leeds LS29JT, UK

O. Sracek
Department of Geology, Faculty of Science,
Palacký University, 17, Listopadu 12, 771 46 Olomouc,
Czech Republic

Introduction

The coal industry in the northeast part of the United Kingdom developed in the thirteenth century. Following a period of intense expansion in the nineteenth and early twentieth century, most of the mines closed between the 1950s and 1990s. Nevertheless, some of the mining relics, such as spoil-heaps, still present a threat to the environment (Environment Agency 2007; Younger et al. 2002). Within spoil tips, sulphide minerals continue to oxidize, generating acid mine drainage (AMD) (Genske 2003; Lee et al. 2002; Sheoran and Sheoran 2006; Younger 2000). Pyrite oxidation causes precipitation of efflorescent salts, e.g. melanterite, rozenite, szomolnokite, romerite, and copiapite (Alpers et al. 1994). The efflorescent salts can immobilize toxic metals within the spoil heap (Dang et al. 2002; Gierè et al. 2003), but they are highly soluble. Their dissolution by recharge water or water level fluctuations sometimes leads to precipitation of more stable minerals, such as members of the jarosite family (Younger 2000), schwertmannite, and iron-oxyhydroxides. Numerous studies have inferred that these phases are the most common precipitates formed during AMD (Bigham et al. 1994; Murad and Rojik 2005; Valente and Gomes 2009).

Efflorescent salts are a highly soluble host for pollutants and thus climatic conditions are crucial in controlling the leachability of these phases. Climatic events and water

Journal : Large 10230 | Dispatch : 25-3-2013 | Pages : 10
Article No. : 223 | LE | TYPESET
MS Code : | CP | DISK

table fluctuations determine the flushing rate and the total amount of sulphate and metals in the water (EPA 1994). In humid climates, the efflorescent salts are rather ephemeral and their dissolution generates a drop in pH and the release of metal ions into solution (Alpers et al. 1994; Hammarstrom et al. 2005). Thus, these supergene phases produced during pyrite oxidation play a key role in controlling metal migration, total sulphate load, and acidity. Efflorescences are indeed indicators of poor water quality (Alpers et al. 2000) and along with the primary sulphide, constitute serious, long-lived source of pollution (Gandy and Younger 2008). Hence, understanding the nature of water–rock interactions during AMD formation and stability of the mineral phases is vital to predict the release of contaminants from weathering spoil.

The Shilbottle spoil heap was created when pyritic shales were excavated and deposited on the surface, covering ca. 15 ha (Fig. 1). Water percolating through the spoil heap causes pyrite oxidation and AMD (Jarvis et al. 2006; Jarvis and Younger 2006). Other sulphides such as arsenopyrite (FeAsS), millerite (NiS), sphalerite (ZnS), and galena (PbS), can oxidize within the spoil heap, adding metals and metalloids such as As, Ni, Zn, and Pb into the solution. Furthermore, a lack of neutralization minerals within the spoil heap permits the generation of highly acidic and metal-rich leachates. Accordingly, the Tyelaw Burn stream, flowing nearby, is contaminated by Al and Fe. A passive treatment system was constructed in an attempt to reduce the contaminant load and to avoid pollution of the River Coquet, which is recharged by Tyelaw Burn and constitutes a site of special scientific interest (SSSI) that is renowned for its salmon fishing. The treatment concept was to intercept seepages polluted mainly by Fe, Al, and sulfate and direct them through a permeable reactive barrier (PRB), where bacterial sulphate reduction (Kemp and Thode 1968; Spence et al. 2001) and the immobilisation of divalent metal ions might take place (e.g. Bottrell et al. 1995). The second part of the treatment system (wetlands) is designed to remove Fe, principally through hydrolysis and precipitation (Jarvis and Younger 2006; Mustafa 2006).

A pE/pH diagram is a useful tool for tracking mineral stability, especially in redox-induced transformations. It has been applied for many years to understand the geochemical behaviour of chemical constituents in water solution (Appelo and Postma 2005; Brookins 1988; Garrels and Christ 1965; Schüring et al. 2000). Recently, pE/pH diagrams have been published for selected components at concentrations typical of AMD (Cravotta 2008; Donahue and Hendry 2003; Espana et al. 2008). These plots represent a classic approach to predict the stability of minerals and aqueous species, i.e. diagrams are divided into separated fields based on the predominance of a certain phase or species. Sometimes, however, these pE/pH diagrams lead

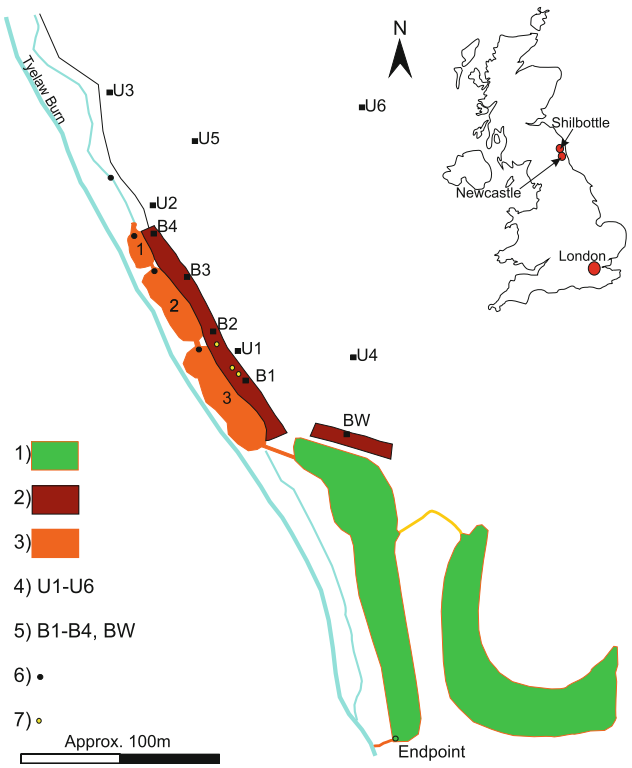

Fig. 1 The study site: *1* aerobic wetland; *2* permeable reactive barrier (PRB); *3* settlement lagoons; *4* observation boreholes within the spoil-heap; *5* observation boreholes within the PRB; *6* sampling points into lagoons, *7* areas of mineralogical probes

to the invalid assumption that physico-chemical conditions occurring within the stability field of the mineral phase must lead to its precipitation. However, the diagram only identifies the most stable phase that might precipitate, while in the natural environment, other competing minerals (in some cases, with a lower saturation index) may form faster and affect the composition of solution (Kölling et al. 2000). Thus, one must remember that the stability diagram does not consider reaction rates.

A few years ago, stability diagrams were developed based on thermodynamic models such as Phreeeqc (Parkhurst and Appelo 1999). Plots can be calculated that account for the complete chemical and physical conditions of the solution. In these diagrams, stability fields of mineral phases often overlap, demonstrating that under certain redox and pH conditions, many minerals may co-occur in the environment. These multi-component diagrams have not become very common, probably because their construction requires both basic programing skills and computational efforts. Multi-component diagrams have been applied to determine the occurrence of trace elements in marine environment (Glasby and Schulz 1999) or to describe chromate transport in a sandy anoxic system containing iron sulphide (Ebert et al. 1997).

Journal : Large 10230 | Dispatch : 25-3-2013 | Pages : 10
Article No. : 223 | LE | TYPESET
MS Code : | CP | DISK

There are a few plots that show the complex geochemistry of highly acidic and metal-rich environments, e.g. for iron-, arsenic- and sulphate-rich water from Wheal Jane Mine in Cornwall (Kinninburgh and Cooper 2004). The diagrams include trace elements such as lithium, arsenic, and zinc, but do not show that a solution may be supersaturated against several mineral phases at the same time. Therefore, we present modified Phreeplot pE/pH diagrams; these plots are constructed using the whole range of dissolved compounds and real physico-chemical conditions, in contrast to the usual diagrams that consider only a few compounds with high concentrations and assume a temperature of 25 °C. In addition, the modified plots illustrate the co-stability of secondary mineral phases, while the classic diagrams show fixed boundaries between phases that suggest their sequential precipitation. This paper couples overlapping multi-phase diagrams constructed using the freeware Phreeplot code with very modest computational efforts and illustrates their application in AMD-affected water. The predictions made on the basis of these plots were compared with observations of the mineralogical composition of cores taken from the studied area (Caraballo et al. 2010), other findings concerning AMD, and analysis of Martian soil samples (Glotch and Rogers 2007; Squyres et al. 2004, 2006).

The modified, site-specific pE/pH diagrams can better represent the detailed mineralogical paragenesis and predict the sequence of mineral precipitation and co-precipitation and can thus be used in the design of a remediation strategy. For instance, preparing these types of diagrams for different scenarios, e.g. variable physico-chemical conditions expected during treatment, might lead to refinement in the design of a remediation system. Moreover, the visualization of the stability fields under real physico-chemical conditions can help to detect shortcomings in operating treatment systems.

Materials and Methods

This paper is based on chemical water analyses performed from 2002 to 2008. Eight wells (U1–U8) within the spoil heap were sampled by pumping water out of the wells through a plastic tube. Samples were collected in pre-washed polyethylene bottles volume of 125 mL. One set of the bottles was pre-acidified with concentrated nitric acid; this set was subsequently divided into two subsets. In the first, water samples were filtered using 0.2 μm cellulose nitrate filters; the second set was unfiltered. The unacidified water samples were used for anion analysis, while the acidified samples were used for cation analysis. Samples were stored in an ice chest and transported to the lab, where they were refrigerated until analysed.

Measurements of water temperature, pH, Eh, electrical conductivity (EC), and alkalinity were made in the field using a Myron 6P Ultrameter (calibrated prior to each monthly sampling) and a Hach Digital Titrator (alkalinity). Alkalinity was determined by titration with sulphuric acid using bromcresol-green methyl-red indicator powder (results are given in mg/L $CaCO_3$). Total concentrations of Cl, SO_4, Ca, Mg, Na, K, Fe, Mn, Al, and Si were determined in the laboratory. Metals were determined using a Varian Vista-MPX ICP-OES, ferrous iron was determined by spectrophotometry using 1,10-phenanthroline indicator (Faulkner et al. 1999), and anions were analysed using a Dionex 110 ion chromatograph. Duplicate samples were collected in accordance with QA/QC procedures. The precision of water analyses was within ±5 %.

The pE/pH diagrams for Fe were constructed using average concentrations of elements such as: Na, Cl, Ca, Mg, K, Fe, Mn, Al, C, Zn, along with sulphate and silica. The lines on the diagrams reflect saturation indices equal to 0 for any mineral phase. It means that within the area delimited by the lines, saturation index (SI) values for a mineral are higher than 0, suggesting it should precipitate. Outside of this area, SI values are less than 0 and the mineral will dissolve until equilibrium is reached. The calculations were performed using the Phreeplot programme (Kinninburgh and Cooper 2011) and the Wateq4f thermodynamic database (Ball and Nordstorm 2001). The computation was carried out over a pH range of 2–12. The final plots were constructed in Excel by extracting data for each mineral phase from the output files.

To present the full spectrum of the mineral assemblage, a new mineral phase was added into the calculations. Schwertmannite, $Fe_8O_8(OH)_{4.8}(SO_4)_{1.6}$, was identified as being associated with AMD in the early 1990s (Bigham et al. 1990, 1994). It often precipitates from sulphate-rich effluents in the pH range of 3–4.5 (Bigham et al. 1996; Gagliano et al. 2004; Jönsson et al. 2005) and generates an ochreous suspension (a.k.a. yellow boy) with other iron minerals.

The application of the dissolution reaction (1) and thermodynamic data for mineral phases not included in the database (K_{eq}) (Majzlan et al. 2004) enables a stability field for this phase to be delineated, corresponding to conditions occurring within the spoil heap.

$$Fe_8O_8(OH)_{4.8}(SO_4)_{1.6} + 20.8H^+ \leftrightarrow 8Fe^{3+} + 1.6SO_4 + 12.8H_2O \quad (1)$$

Given the high concentrations of Al and Si in water within the spoil-heap, the iron aluminosilicate, Fe-berthierine was also added to the interpretation. The occurrence of this mineral was reported in Durham (Smith and Hardy 1981) and in the Cleveland Ironstone Field

Journal : Large 10230 | Dispatch : 25-3-2013 | Pages : 10
Article No. : 223 | LE | TYPESET
MS Code : | CP | DISK

(Younger 2002). It usually formed at low Eh values above a pH of 5 and it has been inferred that Fe-berthierine might be produced where pyrite and kaolinite are both weathering; both minerals have been found within the area adjacent to the spoil heap (Caraballo et al. 2010). This reaction is reversible and proceeds as follows (Fritz and Toth 1997):

$$2FeS_2 + 20H_2O + 28FeOOH + 15Al_2Si_2O_5(OH)_4 \leftrightarrow 15Fe_2Al_2SiO_5(OH)_4 + 15H_4SiO_4 + 8H^+ \quad (2)$$

By using the dissolution reaction (3) and the reaction equilibrium constant (K_{eq}) of $10^{25.55}$, a stability field for Fe-berthierine has been calculated. The pE, which is related to Eh, was estimated from Eq. (4), where Fe^{2+} stands for the concentration of divalent iron.

$$Fe_2Al_2SiO_5(OH)_4 + 10H^+ \rightarrow 2Fe^{2+} + 2Al^{3+} + H_4SiO_4 + 5H_2O \quad (3)$$

$$pE = 17.14 - \log\left(Fe^{2+}\right) - 3pH \quad (4)$$

Results and Discussion

Water Chemistry

The lowest pH value, 2.93, was measured in borehole U6, whereas the highest value, detected in U8, was 7.44 (Table 1). The calculated pE values for water from the spoil-heap ranged between −0.25 and 8.43.

The amount of dissolved sulphate in the spoil heap water ranged from 650 mg/L in U3 to 77,205 mg/L in U6. Iron concentrations ranged from 0.2 to 6,646 mg/L. The amount of dissolved Al within the spoil heap ranged from 0 to 2725 mg/L. High Fe, Al, and sulphate are typical of AMD and are a result of sulphide oxidation and dissolution of Al-bearing minerals at low pH (Fig. 2).

Stability Diagrams for Iron

It is well-known that jarosite forms at pH < 3 when sulfate concentrations are high, schwertmannite is the most common phase precipitating between pH 3 and 4.5 (Bigham et al. 1996), and goethite precipitates at circumneutral pH, usually during recrystallization of ferrihydrite (Schwertmann and Carlson 2005) (Fig. 3). Fe-berthierine occurs at pH > 5, at low Eh conditions, and extremely low sulfate concentrations (Fritz and Toth 1997) (Fig. 3). Thus, general knowledge about the stability of iron minerals indicates that these phases occur in an order and whilst physico-chemical conditions are changing, a single phase should be substituted by another, although many recent AMD examples show that stable and semi-stable minerals are found in this same samples. This may be the effect of partial transformations caused by changing conditions (Elwood Madden et al. 2012; Farrand et al. 2009; Norlund et al. 2010). However, it is also possible that these phases are just more durable than was hitherto stated and their metastability may be much broader.

Figures 4 and 5 represent pE/pH diagram for iron. Plots were calculated for the average chemical composition of water within the spoil-heap. The distribution of iron concentrations indicates heterogeneity. The differences reflect the measured pH values and the oxidation–reduction potential (ORP), i.e. the pE values calculated using Eq. (4). The cluster of points situated in the higher pH area corresponds to water characterised by lower concentrations of iron, i.e. not exceeding 300 mg/L, whereas points on the left part of the diagram reflect very high concentrations of iron, up to 6,600 mg/L.

Precipitating iron(III) minerals are a key driver of AMD water quality (Acero et al. 2006; Sullivan and Bush 2004). Phases usually associated with AMD include jarosite [$KFe_3(SO_4)_2(OH)_6$], goethite [α-FeOOH], ferrihydrite [$Fe(OH)_3$], and schwertmannite [$Fe_8O_8(OH)_{4.8}(SO_4)_{1.6}$] (Schwertmann et al. 1995; Bigham et al. 1996; Gagliano et al. 2004). In addition, as already discussed, Fe-berthierine was also incorporated in the computations.

According to Phreeplot-made diagrams constructed using realistic conditions, jarosite is stable at a pH between 2 to ca. 9, schwertmannite can occur when the pH is in the range of 3–12, whereas goethite is stable over the pH range from 2 to 12. Fe-berthierine is characterized by a rather unusual stability field; at low ORP, it might occur when the pH is greater than 8, while increasing ORP shifts its stability to lower pH values.

Thus, Phreeplot-made diagrams reveal that stability fields of several phases might be much broader than hitherto identified. Hence, one might infer that all of these phases might be present at the same time, and variable and extreme conditions might not favor their complete dissolution. Numerous recent studies indicate that schwertmannite is apparently metastable with respect to goethite; thus, both phases are often present in AMD precipitates (Bigham et al. 1996; Gagliano et al. 2004; Murad and Rojik 2005; Schwertmann and Carlson 2005). This is also consistent with the pE/pH diagram (Fig. 5). The transformation of schwertmannite into goethite through hydrolysis might occur over time scales of weeks to years, according to reactions (5) and (6) (Acero et al. 2006; Regenspurg 2002):

$$Fe_8O_8(OH)_{5.5}(SO_4)_{1.25} + 2.5H_2O \rightarrow 8FeOOH + 2.5H^+ + 1.25SO_4^{2-} \quad (5)$$

$$Fe_8O_8(OH)_6SO_4 + 2H_2O \rightarrow 8FeOOH + 2H^+ + SO_4^{2-} \quad (6)$$

A few studies have indicated that the rate of this transformation is driven by physico-chemical conditions,

Journal : Large 10230 | Dispatch : 25-3-2013 | Pages : 10
Article No. : 223 | LE | TYPESET
MS Code : | CP | DISK

Table 1 Descriptive statistics (minimum, maximum. and average values, along with standard deviation and number of samples) for water sampled within the Shilbottle spoil heap during the years 2002–2008; all concentrations are in mg/L, electrical conductivity (EC) is in µS/cm, and Eh was measured in mV

Site	Stats.	Cl	SO_4	Ca	Mg	Na	K	Fe	Fe^{+2}	Fe^{+3}	Mn	Al	pH	EC	Eh
U1	Min.	13	1,663	256	166	22	6.6	0.6	1.5	0	3.1	9.8	3.19	2,472	67
	Max.	130	15,655	602	1,756	148	20.3	842	842	78	227	862	4.77	11,560	509
	Avg	45.1	5,897	448	665	60	13.4	270.1	399	25	78.7	202.2	4	5,370	268
	SD	27.3	3,739	66	473	38.1	3.8	274.6	259	26	75.4	199.4	0.28	2,539	91
	No.	58	57	54	54	54	54	58	23	23	58	58	57	57	57
U2	Min.	36	2,205	373	805	170	6.6	250	250	0	62	87.3	3.7	5,258	229
	Max.	198	10,720	461	1,033	205	11.4	587	537	84	187	311	4.35	9,544	296
	Avg	71	7,082	423	899	189	9	353	346.3	14	110	163.4	4.02	7,177	257
	SD	42.7	1,995	30	68	10.8	1.6	104.6	90.2	25.4	35.8	78.2	0.2	1,243	20
	No.	14	14	10	10	10	10	14	13	13	14	14	14	14	14
U3	Min.	19	650	382	753	130	16.7	9.8	21.2	0	39.4	8.3	3.6	5,600	138
	Max.	260	8,500	467	1,186	180	53.9	304	288	16	106	230	4.8	7,426	390
	Avg	56	6,078	423	987	152	34.9	86.5	97.5	3	58.4	82.3	4.2	6,701	265
	SD	53.6	1,487	21.3	129.7	12.1	9.2	69.4	80.3	4.2	18.2	68.5	0.34	514	50
	No.	23	23	19	19	19	19	23	13	13	23	23	16	16	16
U4	Min.	22	3,008	444	479	95.2	4	0.2	0.2	0	3.2	0.5	5.92	4,354	−6
	Max.	130	4,580	644	807	345	13.7	24.9	24.9	4.2	12.2	13.8	6.61	5,795	290
	Avg	46.1	3,494	567	654	120.1	6.5	8.2	6.1	1.2	8.5	7.8	6.37	5,282	128
	SD	30.3	366	57.8	106.3	58.3	2.6	6.8	6.8	1.5	2	9.4	0.15	413	83
	No.	20	20	19	19	19	19	20	11	11	20	20	20	20	20
U5	Min.	18	2,564	460	375	126	4.2	3.5	12.3	0	3.6	2.2	5.67	4,285	−41
	Max.	146	6,600	674	869	410	9.4	293	291	4.9	1,500	120	6.85	6,770	269
	Avg	44.8	3,375	579	451.6	345	6	41.4	45.1	1.7	99.4	29.1	6.57	5,135	74
	SD	31.1	898	62	124.5	70.2	1.8	68.2	81.9	1.4	373.5	37.2	0.27	566	98
	No.	16	16	15	15	14	15	16	11	11	16	16	16	16	16
U6	Min.	24	15,693	412	2,359	230	3.9	718	3,321	0	506	257	2.93	3,661	99
	Max.	5,000	77,205	606	10,144	657	13.1	6,646	6,646	625	1,705	2725	4.05	37,180	350
	Avg	411	48,544	486	6,435	354.6	9.35	4,115	4,865	78.1	1,206	1,407	3.56	24,205	259
	SD	1,186	19,095	63.9	2,579.9	126.4	2.47	1,765	1,292.4	221	388	824	0.39	10,658	76
	No.	18	18	17	17	16	17	18	8	8	18	18	18	18	18
U7	Min.	12	3015	427	416	47.6	2.6	52	48.4	3.6	54.7	19.8	2.98	3,818	50
	Max.	100	8,363	988	876	90.9	25.5	587	127	34.5	156	907	6	6,786	444
	Avg	38.8	4,223	565	504	71.1	11.1	168.7	85.9	14.2	82.6	221	4.93	4,628	203
	SD	25.9	1,252	137.5	101.1	13.5	5	145.4	25.4	10	23.3	282.2	0.89	656	99
	No.	20	20	19	19	18	19	20	11	11	20	20	20	20	20
U8	Min.	26	1,270	444	137	63.1	12.6	1.5	0.3	1.1	8.2	0	6.17	2,677	30
	Max.	123	2,514	636	200	88.7	28.2	34.4	18.2	3.9	64.6	28	7.44	3,310	255
	Avg	51	1,616	529	164	74.2	16.6	12.1	4.5	2.6	24.2	7.1	6.68	2,905	156
	SD	26.6	277.2	53.5	17.6	7	3.9	11	5.5	1	15.1	8.2	0.29	199	62
	No.	16	16	15	15	14	15	16	9	9	16	16	16	16	16

Please note that Fe^{2+} and Fe^{3+} concentrations were only measured between 2002 and 2004, while total Fe was determined for the entire period (2002–2008)

i.e. it increases with pH and temperature (Jönsson et al. 2005; Schwertmann and Carlson 2005), and decreases with increasing concentrations of sulphate and dissolved organic carbon (Knorr and Blodau 2007). Moreover, the alteration might occur under anoxic conditions (Burton et al. 2008). The pE/pH diagram representing stability of these phases (Fig. 5) indicates that both phases are stable under similar pH and redox conditions; hence, they might co-occur and

Journal : Large 10230 Dispatch : 25-3-2013 Pages : 10
Article No. : 223 LE TYPESET
MS Code : CP DISK

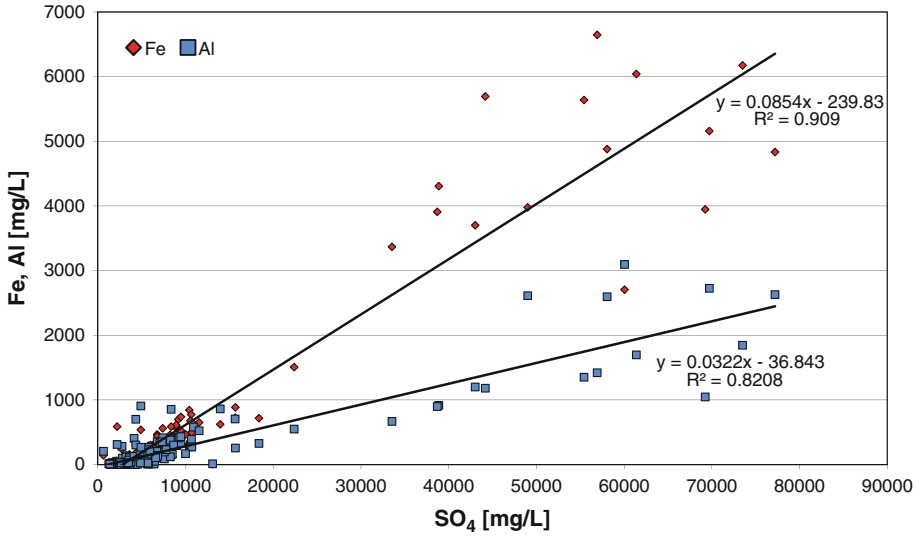

Fig. 2 The relationship between dissolved iron, aluminium, and sulphate in water of the spoil heap

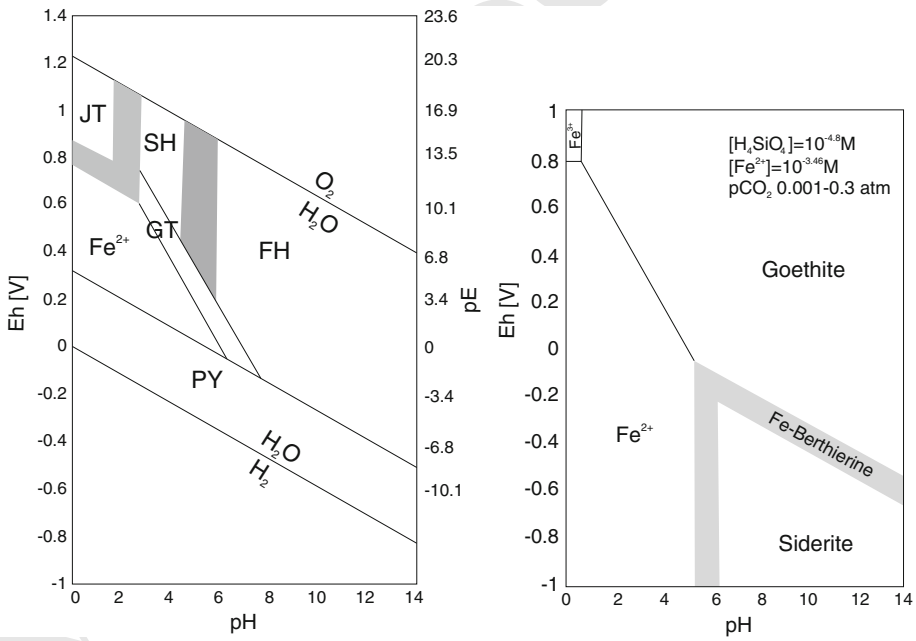

Fig. 3 The Eh–pH diagram on the *left* (after Bigham et al. 1996) shows the stability field of schwertmannite (*SH*) relative to ferrihydrite (*FH*), K-jarosite (*JT*); and goethite (*GT*). The *shaded areas* represent fields of SH and JT metastability, respectively. The Eh–pH diagram on the *right* shows the stability of Fe-berthierine, goethite, and siderite (after Fritz and Toth 1997)

undergo transformations. However, at circumneutral pH and an Eh between −100 and ≈200 mV, schwertmannite should be transformed into goethite.

Recently performed batch dissolution experiments under acidic pH (2) and slightly alkaline pH (8) with jarosite indicate that both dissolution reactions are incongruent. Moreover, a non-ideal dissolution of the parent solid at pH 8 leads to goethite precipitation, which forms a crust on the surface of jarosite grains (Smith et al. 2006). The whole process might proceed according to reaction 7.

$$KFe_3(SO_4)_2(OH)_6 \rightarrow K^+ + 2SO_4^{2-} + 3FeOOH + 3H^+ \quad (7)$$

Thus, over time, not only schwertmannite but also jarosite can be replaced by goethite. Other studies have brought some additional intriguing results concerning the stability of jarosite that incorporate biogenic and non-biogenic sulphur (Norlund et al. 2010). The stability of aerobic biogenic jarosite seems to extend into the schwertmannite field. Indeed, this type of jarosite is stable even at pH 5 and a redox potential of 300–800 mV. While anaerobic biogenic S jarosite is stable under variable conditions, its stability field has been extended into the goethite field and into the field where Fe and S occur as dissolved species.

Summarizing, it is almost certain that boundaries between phases related to AMD are not fixed. Mineral phases can occur simultaneously because their mutual metastability is broader than previously assumed. This has

Journal : Large 10230 Dispatch : 25-3-2013 Pages : 10
Article No. : 223 LE TYPESET
MS Code : CP DISK

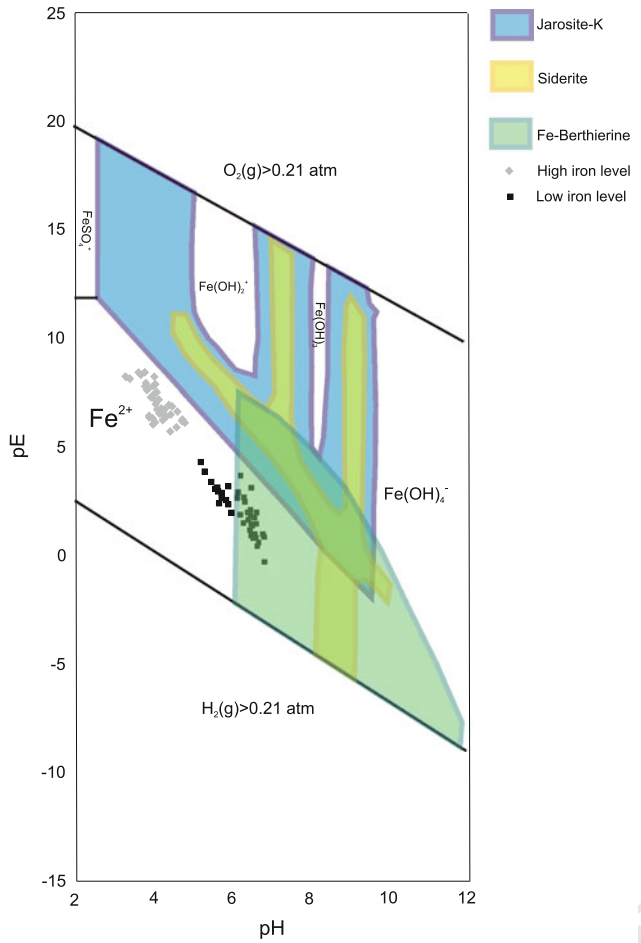

Fig. 4 Stability diagram for selected Fe-phases; minerals are displayed with Fe-species and points representing pH measured in observation boreholes and pE calculated on the basis of Fe^{+2} concentrations. Concentrations (mg/L) of chemical species: Na–144.4, Cl–50.4, S–4537.9, Ca–504.7, Mg–617.9, K–13.9, Fe–134.2, Mn–65.9, Al–101.8, C–258, Zn–1.37, Si–28

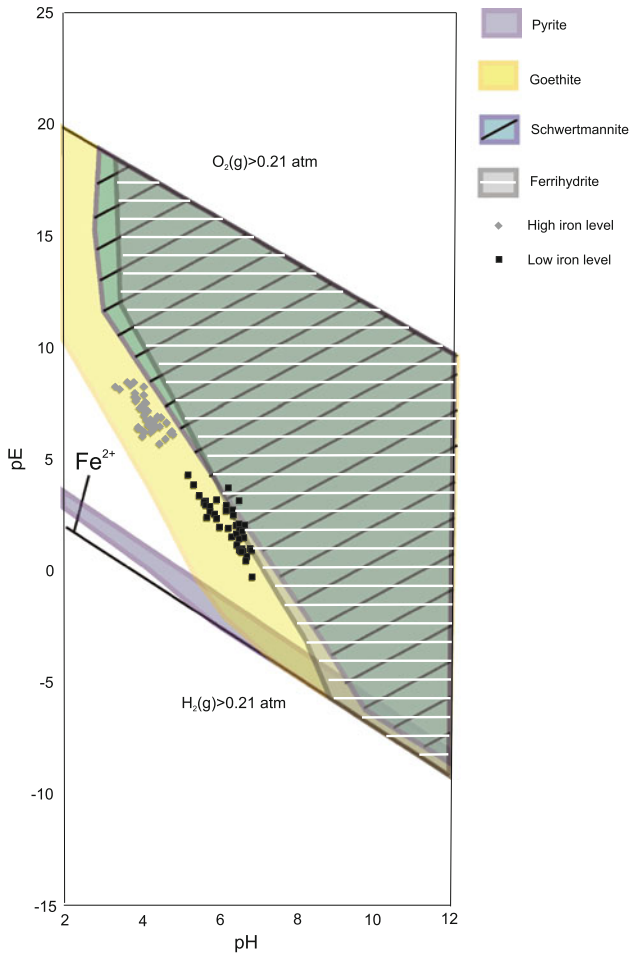

Fig. 5 Stability diagram for selected Fe-phases including goethite; minerals are displayed with Fe-species and points representing pH measured in observation boreholes and pE calculated on the basis of Fe^{+2} concentrations. Concentrations (mg/L) of chemical species: Na–144.4, Cl–50.4, S–4537.9, Ca–504.7, Mg–617.9, K–13.9, Fe–134.2, Mn–65.9, Al–101.8, C–258, Zn–1.37, Si–28

been confirmed by laboratory and field research. For instance, the Martian ferrous and ferric iron research indicate that ferric sulphate and oxides are in close association with each other as well as other sulphate minerals (Farrand et al. 2009; Glotch and Rogers 2007; Squyres et al. 2004, 2006). Analysis of terrestrial examples have also shown that secondary post-mining minerals may be found closely associated, and their metastability fields are variable and usually much broader than expected (French et al. 2012; Herbert 1997; Valente and Gomes 2009). Moreover, in previous studies of the Shilbottle site, mineralogical analysis (XRD analysis and sequential extraction) confirmed the simultaneous presence of schwertmannite, goethite, and ferrihydrite in samples taken from the area adjacent to the spoil heap (Caraballo et al. 2010).

As already mentioned, the Shilbottle site is characterised by both low and high concentrations of iron. The range between these values appears to reflect the stability field of siderite, which suggests that this phase might be a sink of iron at higher pH, according to reaction (8), (Blowes et al. 2003; Coleman et al. 1993; Fig. 4).

$$Fe^{2+} + HCO_3^- \rightarrow FeCO_3 + H^+ \quad (8)$$

In turn, high concentrations of iron are probably the result of secondary sulphate (jarosite, schwertmannite) dissolution, since none of these phases are stable under low pH conditions (Figs. 4, 5). Both phases might also be transformed into goethite, which is very probable considering literature sources and XRD analysis (Caraballo et al. 2010). Hence, low concentrations of Fe

Journal : Large 10230 Dispatch : 25-3-2013 Pages : 10
Article No. : 223 LE TYPESET
MS Code : CP DISK

might also be caused by the replacement of sulphate minerals by goethite, not just increasing pH.

Summary and Conclusions

Supergene minerals produced during pyritic waste oxidation commonly includes ephemeral, highly soluble efflorescent salts and more stable minerals such as jarosite, schwertmannite, and iron-oxyhydroxides. Efflorescent AMD-precipitates play a key role in controlling acidity and sulphate concentrations and metal mobilization in the vicinity of spoil heaps. In addition, their dissolution leads to precipitation of more stable sulphate minerals such as jarosite and schwertmannite. The results of research carried out in the 1990s (Bigham et al. 1996) led to the conclusion that phases connected to AMD are transformed in the order jarosite → schwertmannite → goethite. The constructed classic pE/pH diagrams for iron minerals and simplified physico-chemical conditions confirmed this sequence and reinforced the misconception that physico-chemical conditions that occur within the stability field of the goethite phase must lead to its precipitation.

However, the boundaries between the mineral phases are neither fixed nor narrow. This research illustrated through construction of modified pE/pH diagrams that the solid phases associated with AMD can co-occur and be mutually altered. Moreover, transformations can go in either direction; thus, some alterations might be reversible given changeable physico-chemical conditions, e.g. schwertmannite might be transformed into goethite or jarosite, and jarosite might be replaced by goethite or schwertmannite.

The pE/pH diagrams rely on published kinetic data but since knowledge of the stability of AMD mineral phases is still evolving, the boundaries between minerals cannot yet be definitively fixed. Establishing stability fields of AMD minerals and making a prognosis based only on pE/pH diagrams could be fraught with uncertainty. However, tests of the Phreeplot and Phreeqc codes under various AMD conditions indicate that the stability fields of different phases are similar at very high contaminant concentrations.

Constructed pE/pH diagrams that consider AMD conditions fit well with recently obtained results concerning the co-existence of many post-mining secondary iron minerals. The distribution of points representing observed pE and pH might facilitate further interpretation of hydrogeochemical processes within the AMD environment. For instance, low concentrations of iron within the Shillbottle spoil heap might be the result of siderite precipitation or the transformation of secondary sulphate (jarosite, schwertmannite) into more stable goethite. Stability fields in the diagrams presented will be similar for other cases with very high iron and sulphate loadings and, because the modified diagrams encompass a large set of minerals, they can be used for tracking water–rock interactions in other AMD studies and to address water quality issues. For instance, they might serve as a simple, first approach for checking whether physico-chemical conditions are favourable for leaching of iron and sulphate ions or whether immobilisation of those ions is possible. Moreover, in the case of a passive treatment system, such as at Shillbottle, one might delineate the physico-chemical conditions that would allow the contaminant load to be decreased, e.g. by precipitation of sulphidic minerals (though very narrow stability fields can make this relatively hard) or siderite (possible under slightly alkaline to alkaline conditions).

Further research might include the construction of diagrams for other compounds and conditions selected to reflect a remediation strategy or various kinetic constraints. The reliability of constructed diagrams should be supported by mineralogical examinations of the mineral assemblages.

Acknowledgments This work was funded by the 6th EU project Coal Mines Sites for Targeting Remediation Research (CoSTaR). The authors thank Prof. Paul Younger and Dr Adam Jarvis for their cooperation and especially Ms. Jane Davis for her assistance during our participation in the CoSTAR project at the University of Newcastle. The authors also thank the anonymous reviewers for their valuable comments and Dr. Kleinmann for his editing.

References

Acero P, Ayora C, Torrento C, Nieto JM (2006) The behaviour of trace elements during schwertmannite precipitation and subsequent transformation into goethite and jarosite. Geochim Cosmochim Acta 70:130–4139

Alpers CN, Blowes DW, Nordstrom DK, Jambor JL (1994) Secondary minerals and acid-mine water chemistry. Short course handbook on environmental geochemistry of sulfide mine wastes. Mineralogical Assocation of Canada, Waterloo, pp 247–270

Alpers CN, Jambor JL, Nordstrom DK (eds) (2000) Sulfate minerals—crystallography, geochemistry, and environmental significance. Rev Mineral Geochem 40:608

Appelo CAJ, Postma D (2005) Geochemistry, groundwater and pollution. CRC Press, Boca Raton

Ball JW, Nordstorm DK (2001) User's manual for WATEQ4F, with revised thermodynamic data base and test cases for calculating speciation of major trace, and redox elements in natural water. USGS open-file report 91–183, Washington, DC

Bigham JM, Schwertmann U, Carlson L, Murad E (1990) A poorly crystallized oxy hydroxysulfate of iron formed by bacterial oxidation of Fe(II) in acid minewater. Geochim Cosmochim Acta 54:2743–2758

Bigham JM, Carlson L, Murad E (1994) Schwertmannite, a new iron oxyhydroxy-sulfate from Pyhasalmi, Finland and other localities. Mineral Mag 58:641–648

Bigham JM, Schwertmann U, Traina SJ, Winland RL, Wolf M (1996) Schwertmannite and the chemical modelling of iron in acid sulfate waters. Geochim Cosmochim Acta 60:2111–2121

Blowes DW, Ptacek CJ, Jambor JL, Weisener CG (2003) The geochemistry of acid mine drainage. In: Lollar BS (ed) Environmental geochemistry, treatise on geochemistry 9:149–204

Journal : Large 10230 | Dispatch : 25-3-2013 | Pages : 10
Article No. : 223 | LE | TYPESET
MS Code : | CP | DISK

Bottrell SH, Hayes PJ, Bannon M, Williams GM (1995) Bacterial sulphate reduction and pyrite formation in a polluted sand aquifer. Geomicrobiol J 13:75–90

Brookins DG (1988) Eh-pH diagrams for geochemistry. Springer, Berlin

Burton ED, Bush RT, Sullivan LA, Mitchell DRG (2008) Schwertmannite transformation to goethite via the Fe(II) pathway: reaction rates and implications for iron-sulfide formation. Geochim Cosmochim Acta 72:4551–4564

Caraballo MA, Santofimia E, Jarvis AP (2010) Metal retention, mineralogy, and design considerations of a mature permeable reactive barrier (PRB) for acidic mine water drainage in Northumberland, UK. Am Mineral 95:1642–1649

Coleman ML, Raiswell R, Brown A, Curtis CD, Aplin AC, Ortoleva PJ, Gruszczynski M, Lyons T, Loveley DR, Eglinton G (1993) Microbial mineralization of organic matter: mechanisms of self-organization and inferred rates of precipitation of diagenetic minerals [and Discussion]. Philos Trans R Soc Lond Ser A 344(1670):68–87

Cravotta CA (2008) Dissolved metals and associated constituents in abandoned coal-mine discharges, Pennsylvania, USA, part. 2: geochemical controls on constituent concentrations. Appl Geochem 23:203–226

Dang Z, Congqiang L, Haigh MJ (2002) Mobility of heavy metals associated with the natural weathering of coal mine spoils. Environ Poll 118:419–426

Donahue R, Hendry MJ (2003) Geochemistry of arsenic in uranium mine mill tailings, Saskatchewan, Canada. Appl Geochem 18:1733–1750

Ebert M, Isenbeck-Schröter M, Kölling M (1997) Reduction and retention of chromate in an anoxic quartz-sand-FeS system: a laboratory study in water-saturated columns. In: Ebert M (ed) Der Einfluß des Redox-Milieus auf die Mobilität von Chrom im durchströmten Aquifer, Univ Bremen Ber FB Geowiss 101:70–99

Elwood Madden ME, Madden AS, Rimstidt JD, Zahrai S, Kendall MR, Miller MA (2012) Jarosite dissolution rates and nanoscale mineralogy. Geochim Cosmichim Acta 91:306–321

Environment Agency (2007) River basin planning: summary of significant water management issues, Nortumbria River Basin District. UK Environment Agency, London

EPA (1994) Acid mine drainage prediction. EPA Technical Document 530-R-94-036, NTIS PB94-201829, Washington, DC

Espana JS, Pamo EL, Pastor ES, Ercilla MD (2008) The acidic pit mine lakes of the Iberian Pyrite Belt: an approach to their physical limnology and hydrogeochemistry. Appl Geochem 23:1260–1287

Farrand WF, Glotch TD, Rice JW Jr, Hurowitz JA, Swayze GA (2009) Discovery of jarosite within the Mawrth Vallis region of Mars: implications for the geologic history of the region. Icarus 204:478–488

Faulkner SP, Hintze PE, Ashby SL (1999) Evaluation of colorimetric methods for measuring reduced (ferrous) iron. Water Quality Technical Note PD-02, US Army Corps of Engineers, pp 1–12

French RA, Caraballo MA, Kim B, Rimstidt JD, Murayama M, Hochella MF Jr (2012) The enigmatic iron oxyhydroxysulfate nanomineral schwertmannite: morphology, structure, and composition. Am Mineral 97:1469–1482

Fritz SJ, Toth T (1997) An Fe-Berthierine from a cretaceous laterite. Part 2. Estimation of Eh, pH and pCO2 conditions of formation. Clays Clay Mineral 45(4):580–586

Gagliano WB, Brill MR, Bigham JM, Jones FS, Traina SJ (2004) Chemistry and mineralogy of ochreous sediments in a constructed mine drainage wetland. Geochim Cosmochim Acta 68:2119–2128

Gandy CJ, Younger PL (2008) Predicting long-term contamination potential of preached groundwater in a mine: waste heap using a random-walk method. Hydrogeol J 16:447–459

Garrels R, Christ C (1965) Solutions, minerals and equilibria. Harper and Row, New York City

Genske DD (2003) Urban land degradation investigation remediation. Springer, Berlin

Gierè R, Sidenko NV, Lazareva EV (2003) The role of secondary minerals in controlling the migration of arsenic and metals from high-sulfide wastes (Berikul gold mine, Siberia). Appl Geochem 18:1347–1359

Glasby GP, Schulz HD (1999) Eh, pH diagrams for Mn, Fe, Co., Ni, Cu and As under seawater conditions: application of two new types of Eh, pH diagrams to the study of specific problems in marine geochemistry. Aquat Geochem 5:227–248

Glotch TD, Rogers AD (2007) Evidence for aqueous deposition of hematite and sulfate-rich light-toned deposits in Aureum and Iani Chaos, Mars. J Geophys Res 112:E06001

Hammarstrom JM, Seal RR II, Meier AL, Kornfeld JM (2005) Secondary sulfate minerals associated with acid drainage in the eastern U.S.: recycling of metal and acidity in surficial environments. Chem Geol 215:407–432

Herbert RB (1997) Properties of goethite and jarosite precipitated from acidic groundwater, Dalarna, Sweden. Clays Clay Miner 45:261–273

Jarvis AP, Younger PL (2006) Passive treatment of severely contaminated colliery spoil leachate using permeable reactive barrier. CL:AIRE TDP13:0–48, London

Jarvis AP, Moustafa M, Orme PHA, Younger PL (2006) Effective remediation of grossly polluted acidic, and metal-rich, spoil heap drainage using a novel, low-cost, permeable reactive barrier in Northumberland, UK. Environ Poll 143:261–268

Jönsson J, Persson P, Sjöberg S, Lövgren L (2005) Schwertmannite precipitated from acid mine drainage: phase transformation, sulphate release and surface properties. Appl Geochem 20:179–191

Kemp ALW, Thode HG (1968) The mechanism of the bacterial reduction of sulphate and of sulphite from isotope fractionation studies. Geochim Cosmochim Acta 32:71–91

Kinninburgh DG, Cooper DM (2004) Predominance and mineral stability diagrams revisited. Environ Sci Technol 38:3641–3648

Kinninburgh DG, Cooper DM (2011) PhreePlot. Creating graphical output with Phreeqc

Knorr KH, Blodau C (2007) Chemical controls on schwertmannite transformation. Appl Geochem 22:2006–2015

Kölling M, Ebert M, Schulz HD (2000) A novel approach to the presentation of pe/pH diagrams. In: Schüring J, Schulz HD, Fischer WR, Böttcher J, Duijnisveld WHM (eds) Redox fundamentals, processes and applications. Springer, Berlin, pp 55–63

Lee G, Bigham JM, Faure G (2002) Removal of trace metals by coprecipitation with Fe, Al and Mn from natural waters contaminated with acid mine drainage in the Ducktown Mining District, Tennessee. Appl Geochem 17:569–581

Majzlan J, Navrotsky A, Schwertmann U (2004) Thermodynamics of iron oxides. Part III. Enthalpies of formation and stability of ferrihydrite (~ Fe(OH)3), schwertmannite (~ FeO(OH)3/4(SO4)1/8), and ε-Fe2O3. Geochim et Cosmochim Acta 68:1049–1059

Murad E, Rojik P (2005) Iron mineralogy of mine-drainage precipitates as environmental indicators: review of current concepts and a case study from the Sokolov Basin, Czech Republic. Clay Miner 40:427–440

Mustafa M (2006) Characterisation and modeling of the performance of a novel hybrid passive treatment system for acidic mine drainage. Unpublished PhD thesis, University of Newcastle, Newcastle upon Tyne, UK

Norlund KLI, Baron C, Warren LA (2010) Jarosite formation by an AMD sulphide-oxidizing environmental enrichment: implications for biomarkers on Mars. Chem Geol 275:35–242

Parkhurst DL, Appelo CAJ (1999) User's guide to PhreeqC (version 2): a computer program for speciation, batch reaction, one

Journal : Large 10230 | Dispatch : 25-3-2013 | Pages : 10
Article No. : 223 | LE | TYPESET
MS Code : | CP | DISK

dimensional transport and inverse geochemical calculations, USGS Water Resources Investigations Report 99-4259, Denver, CO, USA

Regenspurg S (2002) Characterisation of schwertmannite; geochemical interactions with arsenate and chromate and significance in sediments of lignite opencast lakes. Unpublished PhD dissertations, University of Bayreuth, Germany

Schüring J, Schulz HD, Fischer WR, Böttcher J (2000) Redox: fundamentals, processes and applications. Springer, Berlin

Schwertmann U, Carlson L (2005) The pH-dependent transformation of schwertmannite to goethite at 25°C. Clay Miner 40:63–66

Schwertmann U, Bigham JM, Murad E (1995) The first occurence of schwertmannite in a natural stream environment. Eur J Mineral 7:547–552

Sheoran AS, Sheoran V (2006) Heavy metal removal mechanism of acid mine drainage in wetlands: a critical review. Miner Eng 19:105–116

Smith FW, Hardy RG (1981) Note clay minerals in the veins of the North Pennine Orefield, UK. Clay Miner 16:309–312

Smith AML, Hudson-Edwards KA, Dubbin WE, Wright K (2006) Dissolution of jarosite [KFe3(SO4)2(OH)6] at pH 2 and 8: insights from batch experiments and computational modelling. Geochim Cosmochim Acta 70:608–621

Spence MJ, Bottrell SH, Thornton SF, Lerner DL (2001) Isotopic modeling of the significance of bacterial sulphate reduction for phenol attenuation in a contaminated aquifer. J Contam Hydrol 53:285–304

Squyres SW, Grotzinger JP, Arvidson RE, Bell JF III, Calvin W, Christensen PR, Clark BC, Crisp JA, Farrand WH, Herkenhoff KE, Johnson JR, Klingelhöfer G, Knoll AH, McLennan SM, McSween HY Jr, Morris RV, Rice JW Jr, Rieder R, Soderblom LA (2004) In situ evidence for an ancient aqueous environment at Meridiani Planum, Mars. Science 306:1709–1714

Squyres SW, Knoll AH, Arvidson RE, Clark BC, Grotzinger JP, Jolliff BL, McLennan SM, Tosca N, Bell JF III, Calvin WM, Farrand WH, Glotch TD, Golombek MP, Herkenhoff KE, Johnson JR, Klingerhofer G, McSween HY, Yen AS (2006) Two years at Meridiani Planum: results from the Opportunity Rover. Science 313:1403–1407

Sullivan LA, Bush RT (2004) Iron precipitate accumulations associated with waterways in drained coastal acid sulfate landscapes of eastern Australia. Mar Freshwater Res 55:727–736

Valente MT, Gomes CL (2009) Occurrence, properties and pollution potential of environmental minerals in acid mine drainage. Sci Total Environ 407:1135–1152

Younger PL (2000) Predicting temporal changes in total iron concentration in groundwaters flowing from abandoned deep mines: a first approximation. J Contam Hydrol 44:47–69

Younger PL (2002) The importance of pyritic roof strata in aquatic pollutant release from abandoned mines in a major, oolitic, berthierine-chamosite-siderite iron ore field, Cleveland, UK. Geol Soc Spec Publ Lond 198:251–266

Younger PL, Banwart SA, Hedin RS (2002) Mine water: hydrology, pollution, remediation. Kluwer, Dordrect

Journal : Large 10230 | Dispatch : 25-3-2013 | Pages : 10
Article No. : 223 | ☐ LE | ☐ TYPESET
MS Code : | ☑ CP | ☑ DISK